

# Ionized Gas in the First 10 Kiloparsecs of the Interstellar Galactic Halo: Metal Ion Fractions<sup>1</sup>

J. Christopher Howk<sup>2</sup>, S. Michelle Consiglio<sup>2,3</sup>

## ABSTRACT

We present direct measures of the ionization fractions of several sulfur ions in the Galactic warm ionized medium (WIM). We obtained high resolution ultraviolet absorption line spectroscopy of post-asymptotic giant branch stars in the globular clusters Messier 3 [ $(l, b) = (42^\circ 2, +78^\circ 7)$ ;  $d = 10.2$  kpc,  $z = 10.0$  kpc] and Messier 5 [ $(l, b) = (3^\circ 9, +46^\circ 8)$ ;  $d = 7.5$  kpc,  $z = +5.3$  kpc] with the *Hubble Space Telescope* and *Far Ultraviolet Spectroscopic Explorer* to measure, or place limits on, the column densities of S I, S II, S III, S IV, S VI, and H I. These clusters also house millisecond pulsars, whose dispersion measures give an electron column density from which we infer the H II column in these directions. We find fractions of  $S^{+2}$  in the WIM for the M 3 and M 5 sight lines  $x(S^{+2}) \equiv N(S^{+2})/N(S) = 0.33 \pm 0.07$  and  $0.47 \pm 0.09$ , respectively, with variations perhaps related to location. With negligible quantities of the higher ionization states, we conclude  $S^+$  and  $S^{+2}$  account for all of the S in the WIM. We extend the methodology to study the ion fractions in the warm and hot ionized gas of the Milky Way, including the high ions  $Si^{+3}$ ,  $C^{+3}$ ,  $N^{+4}$ , and  $O^{+5}$ . The vast majority of the Galactic ionized gas is warm ( $T \sim 10^4$  K) and photoionized (the WIM) or very hot ( $T > 4 \times 10^5$  K) and collisionally ionized. The common tracer of ionized gas beyond the Milky Way,  $O^{+5}$ , traces  $< 1\%$  of the total ionized gas mass of the Milky Way.

---

<sup>1</sup>Based on observations with the NASA/ESA *Hubble Space Telescope* obtained at the Space Telescope Science Institute, which is operated by the Association of Universities for Research in Astronomy, Inc., under NASA contract NAS5-26555. These observations are associated with programs GO9150 and GO9410. Also based on observations made with the NASA-CNES-CSA *Far Ultraviolet Spectroscopic Explorer*. FUSE was operated for NASA by the Johns Hopkins University under NASA contract NAS5-32985.

<sup>2</sup>Department of Physics, University of Notre Dame, Notre Dame, IN, 46556; jhowk@nd.edu

<sup>3</sup>Current Address: Department of Physics and Astronomy, University of California, Los Angeles, Los Angeles, CA 90095, smconsiglio@ucla.edu

## 1. Introduction

Since its discovery in the 1970’s, the origin of the diffuse H $\alpha$  emission arising from the Galaxy has remained something of a mystery (Haffner et al. 2009, Reynolds 1993). This emission, in addition to the free-free radio absorption measurements from the 1960s (see Hoyle & Ellis 1963), implies the existence of a diffuse distribution of free electrons outside of normal H II regions. This warm ionized medium (WIM), often referred to as the “Reynolds Layer” in the Milky Way, dominates the mass of ionized gas in the Milky Way and other galaxies. The power required to keep this gas ionized can be met comfortably only by the Lyman-continuum photon production by early-type stars (Haffner et al. 2009, Reynolds 1993). However, the ionization of this material by OB stars is troublesome: the large scale height of the material ( $\sim 1$  kpc or more; Haffner et al. 1999, Gómez et al. 2001, Gaensler et al. 2008) requires that the photons responsible for ionizing the WIM travel hundreds of parsecs from their point of origin. The large cross-section for absorption of such photons by neutral hydrogen ( $\sigma \sim 6.3 \times 10^{-18}$  cm<sup>2</sup>) naively implies such photons could only travel very small distances, of order 0.1 pc assuming a typical interstellar density ( $\sim 1$  cm<sup>-3</sup>). Various groups have presented models for the ionization of the WIM which rely on photons from hot stars (Mathis 2000; Sembach et al. 2000; Domgörgen & Mathis 1994), photon emission from cooling hot gas (Slavin et al. 2000), heating from magnetic reconnection (Hoffman et al. 2012), and even photons from decaying neutrinos (Sciama 1998).

The hot star ionization models, and to a lesser extent the models invoking cooling hot gas, must assume that the geometry of the interstellar medium (ISM) allows for the propagation of ionizing photons over the large distances required (Miller & Cox 1993, Dove & Shull 1994, Dove et al. 2000, Wood & Mathis 2004, Wood et al. 2010). This includes the concept of density-bounded or “leaky” H II regions (Haffner et al. 2009). In particular, various groups have noted the potential importance of the complicated geometries that may exist in a turbulent, supernova-driven ISM (Miller & Cox 1993, Wood & Mathis 2004), or in superbubbles, where a significant amount of gas has been evacuated about OB associations as a result of correlated supernova explosions (Wood et al. 2010, Dove & Shull 1994, Dove et al. 2000). Coupled with “leaky” H II regions, these geometric considerations may go a long way toward explaining the propagation of ionizing photons from their sources to the WIM gas. However, there is not yet a complete model of the ionization of the WIM, and the predicted ionizing spectrum depends on the assumed sources and the degree to which the photons may be processed through intervening H, thereby modifying the source spectrum (Haffner et al. 2009).

Very sensitive observations of forbidden metal emission lines acquired over the last decade with the Wisconsin H-alpha Mapper (WHAM; Reynolds et al. 1998b; Tufte 1997, Haffner 1999, Madsen et al. 2006) have provided data on the ionization and temperature structure of the WIM (Reynolds et al. 1998a, Haffner et al. 1999, Reynolds et al. 2001, Hausen et al. 2002, Madsen

et al. 2006). Compared with classical H II regions the WIM appears to be warmer (Madsen et al. 2006). Metals and helium in the WIM are generally less highly ionized than in H II regions, as well. In particular, the weakness of forbidden [O III] and He I recombination emission implies relatively low ionization fractions of  $O^{+2}$  and  $He^+$  in the WIM compared with classical H II regions (Reynolds & Tufte 1995, Madsen et al. 2006). Haffner et al. (1999) demonstrated that the ratio of forbidden metal line strengths  $[S \text{ II}]/[N \text{ II}]$  is sensitive to the ionization fraction of  $S^+$ :  $x(S^+) \equiv n(S^+)/n(S)$ . The typical values implied for this ionization fraction in the WIM are  $x(S^+) \approx 0.3 - 0.7$  (Haffner et al. 1999, Madsen et al. 2006). This is higher than seen in O star H II regions where  $S^{+2}$  is more abundant than  $S^+$ . The emission line constraints on WIM ionization imply a lower ionization parameter for the WIM compared to classical H II regions and a distinct spectrum, e.g., due to spectral processing of O star radiation escaping from H II regions and/or contributions from other sources such as cooling radiation (e.g., Slavin et al. 2000) or hot, evolved stars such as white dwarfs (Bregman & Harrington 1986, Haffner et al. 2009, Flores-Fajardo et al. 2011).

While emission line diagnostics have provided some quantitative measures of the WIM ionization, their temperature dependence adds a layer of complexity to understanding the ionization of the medium. Furthermore, because the excitation of these lines relies on collisions with warm electrons, their intensities are weighted by  $\approx n_e^2$ , where  $n_e$  is the electron density, implying they may be strongly weighted toward higher density regions. In this paper we present a complementary approach to probing the ionization state of the WIM. Following Howk et al. (2006) we use ultraviolet (UV) absorption line measures of the multiphase ISM along sight lines to globular clusters that also contain pulsars. The UV observations of post-asymptotic giant branch (PAGB) stars in the background clusters from the *Hubble Space Telescope* (*HST*) and *Far Ultraviolet Spectroscopic Explorer* (*FUSE*) provide measures of metal ion column densities in these directions, while radio observations of pulsar dispersion measures (Hessels et al. 2007) provide determinations of the electron column densities. Taken together we can provide estimates of the ionization fractions of  $S^0$ ,  $S^+$ ,  $S^{+2}$ ,  $S^{+3}$ , and  $S^{+5}$  in the WIM (as well as the total gas phase abundances; see Howk et al. 2006). We apply this technique to two extended sight lines through the Galactic WIM, one probing the first 10 kpc above the disk in the very local region about the sun (Howk et al. 2003, 2006) and the other probing the first 5 kpc of the disk, but some 5 kpc projected radial distance toward Galactic Center (Zech et al. 2008).

The structure of our paper is as follows. In §2 we discuss the methodology underlying our technique, which builds upon the discussion of elemental abundance determinations in Howk et al. (2006). In §3 we discuss the UV absorption line observations, their reduction, and our assessment of the hydrogen and metal column densities along the two sight lines in this work. In §4 we present the results of our analysis of these two sight lines and compare these with previous constraints on WIM physical conditions, while in §5 we discuss the implications of our results and compare them

with theoretical models. We give a summary of our results in §6.

## 2. Methodology

To provide a direct quantitative measure of the ionization fractions of metal ions in the WIM, we rely on unique sight lines that provide measures of both metal ions and neutral hydrogen from UV absorption lines as well as ionized hydrogen from pulsar dispersion measures (DMs). A comparison of the metal ions with the H II column density derived from the pulsar dispersion measures gives the ionization fractions if the abundance of the metal is known.

We write the abundance of a metal  $X$  with respect to H:

$$A(X) \equiv \frac{\sum_j N(X^j)}{N(\text{H I}) + N(\text{H II}) + 2N(\text{H}_2)}, \quad (1)$$

where  $N(X^j)$  is the column density of the  $j$ th ionization stage of  $X$  and the sum is nominally over all ionization states. Thus, the numerator represents the total column density of the metal  $X$ , while the denominator, with  $N(\text{H}) \equiv N(\text{H I}) + N(\text{H II}) + 2N(\text{H}_2)$ , is the total hydrogen column density. In most interstellar absorption line studies,  $A(X)$  is estimated by comparing the dominant ionization state of the element  $X$  in the warm neutral medium (WNM) with the column density of H I. Such studies assume that the neglect of terms in the sums in both the numerator and denominator of Equation 1 has a negligible effect, which is not necessarily true (Sembach et al. 2000), or they attempt to make ionization corrections on the basis of models (e.g., Howk et al. 1999, Howk et al. 2003). Howk et al. (2006) showed that all of the significant terms can be accounted for along sight lines to globular clusters with UV bright stars and radio pulsars. Ultraviolet absorption lines provide measurements of all of the important ionic states of S and sometimes other metals in the WIM and WNM (§3). Those UV measurements combined with the pulsar dispersion measures provide information on all of the states of hydrogen.

Once the abundance is known, the comparison of the column of a metal ion  $X^j$  that arises in the WIM (i.e., with no contribution from the WNM) with the WIM H II column density provides a measure of the ionization fraction of  $X^j$  in the WIM,  $x(X^j) \equiv N(X^j)/N(X)$ . Thus, we can compare the ion  $\text{S}^{+2}$  with the hydrogen reference for the WIM,  $N(\text{H II})_{\text{WIM}}$ :

$$\begin{aligned} \frac{x(\text{S}^{+2})}{x(\text{H}^+)} &= \frac{N(\text{S III})}{N(\text{S})_{\text{WIM}}} \left[ \frac{N(\text{H II})_{\text{WIM}}}{N(\text{H})_{\text{WIM}}} \right]^{-1} \\ &= \frac{N(\text{S III})}{N(\text{H II})_{\text{WIM}}} A(\text{S})^{-1}, \end{aligned} \quad (2)$$

giving a measure of the ionization fraction of  $S^{+2}$  to that of  $H^+$ . Here  $N(S\text{ III})$  does not require the WIM subscript as it arises only within the WIM, with an energy for production that precludes it arising in the WNM. One may write the ionization fractions for  $S^{+3}$  or other WIM ions in a similar way. We can isolate  $x(S^{+2})$  with a value of  $x(H^+) = 0.95 \pm 0.05$  based on observations of the weakness of [O I] emission from the Galactic WIM (Reynolds 1989, Reynolds et al. 1998a, Haffner et al. 2009).

The determination of the H II column in the WIM,  $N(H\text{ II})_{WIM}$ , requires two corrections to the electron column density,  $N(e^-)$ , provided by the DMs (Howk et al. 2006). The first corrects for the contribution to  $N(e^-)$  from hot ionized gas since we cannot measure the S ions found in this hot gas (e.g., S VII and higher). This correction is discussed with the pulsar DMs below in §2.1. The other is the correction for the  $e^-$  contributed to the DM from ionized He. We use the helium ionization correction factor,  $\eta$ , discussed in detail in Howk et al. (2006) such that  $N(H\text{ II}) = \eta N(e^-)$ . In this work we adopt  $\eta_{WIM} = 0.98 \pm 0.01$ , the “minimum helium ionization” case discussed in Howk et al., which assumes the ionization fraction of  $He^{+2}$  in the WIM is minimal. The choice of the minimum or maximum helium ionization correction represents a (small) systematic uncertainty. However, the maximum helium ionization case ultimately produces an inconsistency: we show below (even using the maximum case) that the ionization fraction of  $He^{+2}$  must in fact be very small (§4, §5).

## 2.1. Correcting for the Hot ISM

We estimate HIM contribution to  $N(e^-)$  following the general outline of Howk et al. (2006). We assume the HIM electrons arise in two components, one from  $T \approx 10^5 - 10^6$  K gas traced by O VI the other from  $T > 10^6$  K gas traced by X-ray absorbing/emitting gas. Thus

$$N(e^-)_{HIM} = \eta_{HIM}^{-1} [N(H\text{ II})_5 + N(H\text{ II})_6], \quad (3)$$

where  $N(H\text{ II})_5$  and  $N(H\text{ II})_6$  are the H II columns associated with the  $T \sim 10^{5-6}$  K and  $> 10^6$  K gas, respectively. The helium correction factor is  $\eta_{HIM}$ . In this coronal gas, we assume all of the helium is in the form of  $He^{+2}$ , giving  $\eta_{HIM} = 0.83$  (Howk et al. 2006).

We estimate the first term in brackets from Equation 3 from the O VI column density along the line of sight (Wakker et al. 2003; Savage et al. 2003). We write

$$N(H\text{ II})_5 = \frac{N(O\text{ VI})}{A(O)x(O^{+5})}, \quad (4)$$

where  $N(O\text{ VI})$  is the measured O VI column density derived directly from *FUSE* data (see §3.2),  $A(O) = (4.90 \pm 0.6) \times 10^{-4}$  (Asplund et al. 2009) is the assumed gas-phase oxygen abundance,

and  $x(\text{O}^{+5}) = 0.2$  (Sutherland & Dopita 1993, Savage et al. 2003) is the ionization fraction of  $\text{O}^{+5}$  in this phase of the gas (see discussion in Howk et al. 2006). This is the maximum value found in most models, and some of the gas probed by  $\text{O VI}$  could have an ionization fraction lower by a factor of a few, depending on the conditions probed by the gas. This lower-temperature component is the smallest contributor to the whole, representing  $< 25\%$  of the total HIM column (in our calculations and §4). We adopt a 50% uncertainty on the implied column given the large uncertainties involved.

The  $T > 10^6$  K gas, represented by the second term in brackets from Equation 3, has no direct probe along the specific sight lines studied in this work. Instead, we adopt a mean Galactic distribution for this gas constructed to match X-ray absorption measurements of  $\text{O VII}$ ,  $\text{O VIII}$ , and  $\text{Ne IX}$  (Yao & Wang 2005; Yao et al. 2009). The absorption line measurements are made toward both Galactic and extragalactic objects. The refined model presented in Yao et al. (2009) assumes a thick disk structure described by a single exponential disk,  $n_H(z) = n_H(0) \exp(-|z|/h_z)$ , with a mid-plane density  $n_H(0) = 1.4 \times 10^{-3} \text{ cm}^{-3}$  and scale height  $h_z = 2.8 \text{ kpc}$ . We integrate the  $z$  distribution of hot gas densities to give

$$N(\text{H II})_6 = (\sin |b|)^{-1} \int_0^{z_*} n_H(z) dz \quad (5)$$

with the upper integration limit being the  $z$ -height of the star. This estimate of the HIM column density has many simplifying assumptions whose validities are difficult to assess. As a result, we adopt a 50% uncertainty in our HIM column density estimates.

### 3. Observations, Reductions, and Measurements

In this work we apply the approach outlined above to study the ionization fractions of  $\text{S}^0$ ,  $\text{S}^+$ ,  $\text{S}^{+2}$ ,  $\text{S}^{+3}$ , and  $\text{S}^{+5}$  in the WIM for two directions through the Galactic WIM, those toward the globular clusters M 3  $[(l, b) = (42^\circ 2, +78^\circ 7); d = 10.2 \text{ kpc}, z = 10.0 \text{ kpc}]$  and M 5  $[(l, b) = (3^\circ 9, +46^\circ 8); d = 7.5 \text{ kpc}, z = +5.3 \text{ kpc}]$ . In what follows, we describe the UV data and analysis used to derive the metal and neutral hydrogen column densities along these sight lines (§3.1 through §3.3). We also describe the pulsar dispersion measures and their uncertainties (§3.4).

#### 3.1. UV Observations

In this work we make use of UV spectra from the Space Telescope Imaging Spectrograph (STIS) on board *HST* and from *FUSE* to study the metal ion and H I column densities toward M 3 and M 5. The sight line to M 3 is probed toward the PAGB star von Zeipel 1128 (vZ 1128);

the observations, reductions, and measurements for this sight line have been discussed in Howk et al. (2003, 2006). The ISM toward M 5 is probed along the sight line to the PAGB star ZNG 1; the observations and their reductions have been described by Zech et al. (2008). The latter work specifically studied the high velocity gas along the M 5–ZNG 1 direction. We present the first measurements of the low velocity gas along this sight line here.

The STIS<sup>1</sup> observations used in this work all employed the E140M grating to cover the spectral range  $\sim 1150$  to  $1710$  Å at a resolution  $R \equiv \lambda/\Delta\lambda \approx 45,800$ . This provides measures of the ISM absorption lines at an equivalent velocity resolution  $\Delta v \approx 6.5$  km s<sup>−1</sup> (FWHM). The M 3–vZ 1128 observations (program ID 9150; PI Howk) were obtained with the  $0''.2 \times 0''.06$  aperture. The typical signal-to-noise ratios are in the range  $\approx 20$ – $40$  per resolution element. The M 5–ZNG 1 observations (program ID 9410; PI Howk) were obtained with the  $0''.2 \times 0''.2$  aperture. The two datasets have slightly different line spread function (LSF) shapes, notably differing in the strength of the extended wings of the LSF, due to the different apertures used. The STIS M 5–ZNG 1 data have signal-to-noise ratios  $\gtrsim 25$  per resolution element in the regions of interest for this work (Zech et al. 2008).

The *FUSE* observations used here cover the spectral range  $905$  to  $1185$  Å at a resolution  $R \approx 15,000$  giving a velocity resolution  $\Delta v \sim 20$  km s<sup>−1</sup> (FWHM). The data were all taken through the LWRS  $30'' \times 30''$  apertures, and we have combined observations acquired as part of several programs (Howk et al. 2003, Zech et al. 2008). These data have signal-to-noise ratios  $\gtrsim 20$  per resolution element in the regions of interest. While the wavelength calibration of the STIS data is excellent, the *FUSE* absolute (and to some extent relative) wavelength calibrations are not as well constrained. As discussed in the earlier source papers (Zech et al. 2008, Howk et al. 2006), we have bootstrapped the *FUSE* wavelength scale to match that of the STIS data using both stellar and interstellar lines to determine the alignment.

### 3.2. Metal Ion Column Densities

We use the STIS and *FUSE* observations to derive column densities and limits for several metal species toward M 5–ZNG 1, with the relevant results given in Table 1. We focus on the ions of S, since we have access to absorption from ions that probe the WIM directly (S III and S IV). In addition, we give measurements of the “high ions” Si IV, C IV, N V, and O VI along both sight lines. The O VI is required for estimating the HIM H II column density, but we will eventually use these high ions to understand the ionization fractions of both the WIM and HIM in the Galaxy

---

<sup>1</sup>Proffitt et al. (2002) discuss the STIS instrument characteristics in detail.

(§4).

To determine the metal ion columns we fit the stellar continuum in the regions surrounding metal absorption lines using low order Legendre polynomials. We directly integrate the line absorption profiles and apparent optical depths to determine the equivalent widths and apparent column densities,  $N_a$ , following Sembach & Savage (1992). In all cases we adopt central wavelengths and oscillator strengths from Morton (2003). To calculate the limiting equivalent width and apparent column density of S I, we assume an intrinsic width of  $\sim 30 \text{ km s}^{-1}$  (FWHM), the value derived from a single Gaussian profile fit to the S II 1250.584 Å transition. All limits given in this work are  $3\sigma$ .

Deriving the column densities of S II and S III toward M 5–ZNG 1 required special care. The absorption profiles for all of the transitions from these ions are shown in Figure 6. The integrated apparent column densities derived from the weaker S II transitions at 1250.584 and 1253.811 Å, which have  $f$ -values that are different by a factor of two, differ by  $\sim 0.07$  dex, with the weaker transition giving a higher  $N_a$ . The strongest of the S II lines observed by STIS, at 1259.519 Å and having an  $f$ -value three times higher than the weakest, gives a significantly lower value yet for  $N_a$ . This progression of decreasing  $N_a$  with increasing  $\lambda f$  suggests these lines contain unresolved saturated structure (Savage & Sembach 1991).

Figure 2 compares the apparent column density profiles as a function of velocity,  $N_a(v)$ , for S II  $\lambda 1250$ , 1253, and S III  $\lambda 1190$  (all from STIS). The weakest S II transition (at 1250.584 Å) is shown in each of the two panels as the thin black histogram. The discrepancies between the two S II transitions in the top panel are consistent with expectations in the classical case of unresolved saturation. Since there appears to be only moderate saturation in the S II, following Savage & Sembach (1991) we correct the column density for S II  $\lambda 1250$  based on a comparison with the 1253 transition and adopt an uncertainty appropriate for the uncertainties in the method (the integrated uncertainties in  $N_a(v)$  being minimal). This gives our final adopted value of  $\log N(\text{S II}) = 15.59 \pm 0.10$ . This amounts to an  $+0.07$  dex correction for saturation compared with the value derived from S II  $\lambda 1250$ .

The S III transitions toward M 5–ZNG 1 are both contaminated to varying degrees. S III 1012 is contaminated by adjacent H<sub>2</sub> transitions, while the S III transition at 1190 Å is adjacent to and slightly contaminated by Si II at 1190.416 Å (a velocity offset of  $+52.4 \text{ km s}^{-1}$  with respect to S III). We deal with these contaminations in two separate ways. We correct S III  $\lambda 1190$  for the presence of underlying absorption from Si II  $\lambda 1190$  using an apparent optical depth profile for the Si II derived from the Si II transitions at 1193.290 and 1526.707 Å. In each case we scale the relative  $\lambda f$ -values of the transitions involved in order to estimate the contribution from the 1190.416 Å transition of Si II as a function of velocity. Using these two comparison lines, which differ in strength by a factor of 3.4, leads to the same value for the integrated  $N_a(v)$  profile of S III



$\lambda 1190$ :  $\log N_a(\text{S III}) = 14.66 \pm 0.04$ .

We assess the strength of the  $\text{H}_2$  lines contaminating S III  $\lambda 1012$  following Howk et al. (2002), who discuss this issue for contamination of O VI absorption. We assess the strength of the  $\text{H}_2$  lines contaminating S III  $\lambda 1012$  using lines of similar  $f$ -values arising from the same rotational states. In this case, the derived column density is sensitive to the assumptions about this correction and a somewhat uncertain continuum placement. We derive column densities from S III  $\lambda 1012$  that are significantly lower than those derived from the STIS-observed S III  $\lambda 1190$ :  $\log N_a(\text{S III}) \approx 14.53 \pm 0.05$  to  $14.59 \pm 0.04$  (statistical errors only), depending on the assumptions about the continuum fit, details of the  $\text{H}_2$  contamination correction, and resolution of the *FUSE* channel from which the data are adopted. The smaller columns derived from this weaker line of S III are smaller than those for the stronger line at 1190 Å, suggestive of some unresolved saturation in at least the *FUSE* data. However, given the uncertainties in the measurements of S III  $\lambda 1012$ , it is difficult to directly compare the two values as we did for S II above.

On the other hand, the peak apparent optical depth of S III 1190 as observed with the higher-resolution STIS instrument is only  $\sim 60\%$  that of S II 1250 (including the underlying absorption from Si II 1190). Even though they do not trace exactly the same gas, it is unlikely the S III 1190 transition is saturated to the extent of the S II 1250 transition. This, with the difference in derived  $N_a(v)$  values between the two transitions of S III, limits the required saturation correction for the S III 1190 apparent column density to be  $< +0.07$  dex, the value adopted for S II. The only other comparable probes we have of the low-velocity gas are the Si IV 1393, 1402 Å lines (Zech et al. 2008), which show little to no apparent unresolved saturation for optical depths  $> 2\times$  that of S III. However, while their shape is similar to that seen in S III, they are offset by  $\sim -4 \text{ km s}^{-1}$  and trace a somewhat different mixture of gas than S III.<sup>2</sup> Profile fitting does not ultimately provide a firm assessment of the possible saturation, as there is little information on the intrinsic shape of the S III profile from other transitions, and the  $\text{H}_2$  contamination and unknown LSF that plague the *FUSE* observations of the 1012 Å transition make that approach non-unique in our tests. We proceed by adopting a saturation correction of  $+0.035$  dex and adding a systematic uncertainty of  $\pm 0.035$  linearly to the statistical uncertainties. We adopt this uncertainty under the assumption that the correction should be  $< 0.07$  dex at the  $2\sigma$  level. Our adopted column density is thus  $\log N(\text{S III}) = 14.70 \pm 0.06$ .

Several other metal species are listed in Table 1, which represent more straightforward measurements. *FUSE* observations place stringent limits on the S IV column densities through the 1062.664 Å transition for both sight lines, while we are also able to place limits on S VI toward

---

<sup>2</sup>This appears not to be due to a wavelength calibration uncertainty, as the Si IV high velocity cloud absorption seen in both transitions is consistent at velocities consistent with those seen in Si II 1190.

M 3–vZ 1128 using the doublet at 933.387 and 944.523 Å. For the M 5–ZNG 1 sight line, we are not able to place meaningful limits on S VI given the strong contamination from H<sub>2</sub> in the FUV. Given the column of S IV is well below that of S III toward M 5–ZNG 1, we assume the S VI column would be minimal toward this star as it is toward M 3–vZ 1128. Limits to S I  $\lambda$ 1295.653 absorption from STIS show its column density to be negligible along both sight lines.

### 3.3. Neutral and Molecular Hydrogen Column Densities

We derive the interstellar H I column density of these two sight lines by fitting the damping wings of the Lyman- $\alpha$  profile observed by STIS. For the sight line to M 3–vZ 1128 we adopt the Lyman- $\alpha$  derived H I column density from Howk et al. (2006). Here we determine the H I column density toward M 5–ZNG 1 in an identical manner.

The neutral hydrogen column in the direction of M 5 can be estimated from H I 21-cm emission observations. As noted in Zech et al. (2008), the column density derived from the publicly-available Leiden-Argentine-Bonn (LAB) Survey (Kalberla et al. 2005) is  $\log N(\text{H I}) = 20.56 \pm 0.17$ . This value is averaged over a 36' beam approximately centered on M 5. However, small-scale structure within this large beam can cause this average value to be different than that appropriate for comparison with the pencil-beam measurements of metal ions toward M 5–ZNG 1 itself. We adopt an error following the recommendations of Wakker et al. (2001) for the use of large beam H I 21-cm observations for absorption line studies.

Figure 3 shows the STIS spectrum of the Lyman- $\alpha$  absorption line toward M 5–ZNG 1. The broad Lyman- $\alpha$  absorption is a combination of stellar atmospheric and foreground ISM absorption. We remove the contaminating stellar absorption by using the stellar atmosphere model described in Zech et al. (2008) to normalize the data during our fitting procedure. The model atmosphere was calculated with TLUSTY (Hubeny & Lanz 1995) assuming an effective temperature  $T_{\text{eff}} = 45,000$  K, with  $\log g = 4.48$ , and an atmosphere consisting of 99% He by number (W.V. Dixon, 2007, private communication) with a mix of abundances specified in Zech et al. (2008). The adopted stellar continuum is shown as the blue line in Figure 3. We use a second-order Legendre polynomial to match the model atmosphere to the STIS spectrum. Ideally the model atmosphere should provide a very good estimate of the distribution of flux with wavelength. In practice the models deviate slightly from the spectral energy distribution in the data. Small discrepancies between the model and observations are due to large-scale calibration and small-scale order combination uncertainties in the data and uncertainties in the large-scale flux distribution of the model itself. The polynomial parameters are treated as free parameters during the fitting process and contribute appropriately to the error budget.

The best-fit interstellar H I column density from our modeling of Lyman- $\alpha$  is  $\log N(\text{H I}) = 20.47 \pm 0.02$ . The best-fit profile is shown as the red line in Figure 3. This error estimate is dominated by uncertainties the adopted stellar properties and their affect on the stellar models, which we explore in the fitting process (c.f., Sonneborn et al. 2002).

The molecular hydrogen content for both sight lines is completely negligible compared with the H I and H II columns. The sight line to M 3–vZ 1128 shows no detectable H<sub>2</sub> absorption (Howk et al. 2003), with  $\log N(\text{H}_2) < 14.35$  ( $3\sigma$ ) summed over  $J \leq 3$ . This implies a molecular hydrogen fraction  $\log f(\text{H}_2) \equiv \log 2N(\text{H}_2)/[N(\text{H I}) + 2N(\text{H}_2)] < -5.3$ . Toward M 5–ZNG 1, our *FUSE* data show a forest of moderate strength H<sub>2</sub> transitions. However, none show damping wings, which severely limits the column densities. Deriving the precise column density is not crucial for this sight line, and we use the lack of damping wings and other considerations to limit the column:  $\log N(\text{H}_2) < 18.0$  ( $3\sigma$ ) integrated over  $J \leq 5$  states. This yields  $\log f(\text{H}_2) < -2.4$ . The H<sub>2</sub> contribution to the total hydrogen column along both sight lines is negligible.

### 3.4. Radio Pulsar Dispersion Measures and the Ionized Hydrogen Column Densities

The electron column densities toward M 3 and M 5 are derived from the dispersion measures toward millisecond pulsars in each cluster. Following Howk et al. (2006) we average the dispersion measure for three M 3 pulsars (M 3A, M 3B, and M 3D), giving  $\langle \text{DM} \rangle_{\text{M 3}} = 26.33 \pm 0.15 \text{ pc cm}^{-3}$  (standard deviation). We do not include the unconfirmed pulsar M 3C in this average, although it gives a consistent DM (Hessels et al. 2007). The uncertainties in these DM measurements are very small, typically  $\sim 0.1 \text{ pc cm}^{-3}$  or better. This average dispersion measure is equivalent to an electron column density of  $\log N(e^-) = 19.91 \pm 0.01$  in typical units ( $\text{cm}^{-2}$ ). For M 5 we average the *DM* for the five known millisecond pulsars (Hessels et al. 2007, Freire et al. 2008) giving  $\langle \text{DM} \rangle_{\text{M 5}} = 29.5 \pm 0.3 \text{ pc cm}^{-3}$  (standard deviation) or  $\log N(e^-) = 19.96 \pm 0.01$ . These are the total electron columns, including contributions from the WIM and the HIM along these sight lines.

The application of Equation 3 to the sight lines in this work yields  $\log N(e^-)_{\text{HIM}} \sim 19.08$  and  $19.00 \text{ cm}^{-2}$  for the M 3–vZ 1128 and M 5–ZNG 1 sight lines, respectively (see Table 2). We assume O VI column densities from Table 1. The result for M 3–vZ 1128 is slightly different than that reported in Howk et al. (2006) given the different approach to assessing the contribution from the hottest HIM component,  $N(\text{H II})_6$ , but the difference is small enough that it produces a negligible change in the final results. For example, the  $A(S)$  reported here is different by only  $\sim 0.01$  dex compared with the earlier value. Adopting the Howk et al. methodology for the M 5–ZNG 1 sight line, however, would produce results that differ by  $\sim 0.1$  dex given the greater importance of lower  $z$ -height gas along that sight line.

## 4. Results

The final results of our WIM analysis are presented in Tables 2 and 3. Table 2 gives the physical parameters derived for each of the sight lines, including the hot gas columns, WIM fractions, and  $A(S)$ . Table 3 presents the final ionization fractions for  $S^0$ ,  $S^+$  (see below),  $S^{+2}$ ,  $S^{+3}$ , and  $S^{+5}$  in the WIM for the two sight lines. To derive the ionization fractions, we adopt the S abundance toward M 3, which is much better determined than that toward M 5 and equivalent to the solar system meteoritic abundance. Sulfur does not seem to be depleted by large amounts into dust grains (again evidenced by the solar-like abundance toward M 3), so it is reasonable to assume  $A(S)$  is roughly constant in the solar neighborhood. While the M 5 sight line is toward the inner Galaxy, the majority of the absorption likely occurs within the first  $z < 1$  kpc given the scale height of the WIM, and thus relatively close to the Sun.

The two sight lines in this study may trace different conditions in the WIM. The high-latitude cluster M 3 is close to the Galactic north pole and probes the WIM in a column above the sun. On the other hand, M 5 lies toward the inner Galaxy at  $b \sim +45^\circ$ , probing WIM gas somewhat interior to the solar circle. As shown in Table 2, the mean fractions of ionized gas along the sight lines differ by a factor of  $\sim 2$ . The sight line to M 3 has a total ionized gas fraction  $N(\text{H II})/N(\text{H}) = 0.45 \pm 0.09$ ,<sup>3</sup> whereas that toward M 5 is only  $0.19 \pm 0.03$ . This is likely due in large part to the differing paths through low- $z$  gas associated with the denser, more neutral thin disk of the Galaxy. The M 5 sight line probes a proportionally-larger contribution from the low- $z$  gas.

Within the warm ionized gas, we find ionization fractions  $x(S^{+2}) = 0.33 \pm 0.07$  for M 3 versus  $0.47 \pm 0.09$  for M 5 (Table 3).<sup>4</sup> Here we have transformed from  $x(S^{+2})/x(\text{H}^+)$  assuming a hydrogen ionization fraction  $x(\text{H}^+) = 0.95 \pm 0.05$  to represent the WIM, which generally has  $x(\text{H}^+) > 0.9$  (Reynolds 1989, Reynolds et al. 1998a, Hausen et al. 2002, Haffner et al. 2009). These ionization fractions are column density-weighted averages over the entire sight lines. We do not detect S IV absorption along either sight line, and this absence limits the ionization fraction  $x(S^{+3}) < 0.04$  ( $3\sigma$ ) for both. The ionization fractions of  $S^0$  in the WIM are very low, as expected:  $x(S^0) < 0.004$  ( $3\sigma$ ) along both sight lines.

The ionization fraction of  $S^+$  in the WIM cannot be directly measured through the column density of S II, since that ion contains significant contributions both from the WNM and WIM (with the WNM dominating the column). However, none of the ionization states higher than  $S^{+2}$  contribute significantly to the total, with very stringent  $3\sigma$  limits to the ionization fractions of  $S^{+3}$

---

<sup>3</sup>The values quoted here for the M 3 sight line differ slightly from those of Howk et al. (2006) due to the difference in the treatment of the HIM contribution.

<sup>4</sup>Utilizing the directly measured value for  $A(S)$  toward M 5 yields  $x(S^{+2}) = 0.67 \pm 0.19$ .

and  $S^{+5}$ .<sup>5</sup> Given no higher ionization states are present, the ionization fractions of  $S^+$  and  $S^{+2}$  must sum to nearly unity, i.e.,  $x(S^+) + x(S^{+2}) \approx 1$ . We use this to estimate the ionization fractions of  $S^+$  within the WIM along these sight lines:  $x(S^+) = 0.67 \pm 0.07$  and  $0.53 \pm 0.09$  for M 3 and M 5, respectively (allowing for a  $1\sigma$  contribution from  $S^{+3}$  in the error budget).

The distribution of S ion fractions in the WIM as a function of ionization energy is shown in the top panel of Figure 4 for  $S^0$  through  $S^{+5}$  (excluding  $S^{+4}$ ), with values for the M 3 and M 5 sight lines shown in black and red, respectively. The horizontal bars for each ion span the creation to destruction energies for each ionization state. On the whole the results from the two sight lines are in good agreement. There is a strong peak in the ion fractions for energies between  $\sim 10$  and 35 eV, with very little at higher energies. On the whole the two sight lines give a consistent picture of the ionization distribution. The M 5 sight line may slightly favor  $S^{+2}$  compared with that to M 3, but any variations are at less than  $2\sigma$ .

Independent information on the metal ion fractions in the WIM can be derived from emission line observations. Results derived from such studies are compared with ours in Figure 5. Haffner et al. (2009) give a recent review of WIM emission line observations and physics (both for the Galactic WIM and the diffuse ionized gas in external galaxies). They combine the observations of Haffner et al. (1999) and Madsen et al. (2006), who used WHAM to observe forbidden metal line emission from the diffuse Galactic WIM. Their observations of the ratio  $[S \text{ II}]/H\alpha$  provide a measure of  $x(S^+)$  when the temperature can be estimated with observations of  $[N \text{ II}]/H\alpha$  (Haffner et al. 1999). As summarized in Haffner et al. (2009), the WHAM results give  $x(S^+) \sim 0.3$  to 0.7, with the majority of the sight lines seemingly above 0.5. The results for the two sight lines studied here, giving  $x(S^+) \sim 0.5$  and 0.7, are completely consistent with the WHAM estimates (Figure 5).

The lack of S IV and higher ion absorption is also consistent with WHAM observations of forbidden  $[O \text{ III}]$  emission from the WIM, which show  $x(O^{+2}) \lesssim 0.1$  in all cases and  $< 0.05$  for a majority of the diffuse gas (Madsen et al. 2006). O III probes a range of ionization energies 35.12 to 54.93 eV, similar to those probed by  $S^{+3}$  (see Figure 5). Similarly, observations of He I recombination radiation limit the ionization fraction of singly-ionized helium. Observations find ionization fractions of singly-ionized helium as high as  $x(He^+) \lesssim 0.6$ , although many sight lines have  $x(He^+) \lesssim 0.3$  or so (Madsen et al. 2006; Reynolds & Tufte 1995). Given the lack of higher ionization states of S from our results, the remainder of the He is likely to be neutral (see §5).

There seems to be a significant amount of variation in the  $O^{+2}$  and  $He^+$  ionization fractions with location in the Galaxy. The highest ionization fractions from Madsen et al. (2006) in particular

---

<sup>5</sup>While we do not have a probe of  $S^{+4}$ , the lack of significant quantities of any other species with ionization energies  $\gtrsim 35$  eV (in the WIM or the hot gas up to  $\gtrsim 150$  eV; see below), we do not expect  $S^{+4}$  to be present in significant amounts.

seem to be found associated with energetic regions very near the disk or in unusual filaments. The diffuse WIM and even supershells tend to trace the lower end of these ionization fractions. Figure 5 shows the full range of observed values, from the lowest upper limits (shown with downward pointing arrows) to the more extreme, higher ionization sight lines (Madsen et al. 2006). However, on the whole the emission line observations paint a similar picture to our absorption line study: ions requiring  $> 35$  eV for production make a relatively small contribution to the total.

While we have concentrated to this point on the ionization fractions within the WIM, we also have an opportunity along these sight lines to consider the ionization fractions of a broad range of ions in the total ionized gas of the Milky Way (i.e., WIM+HIM). Here we write the total column density of H II as

$$N(\text{H II}) = [(1 - f_{\text{HIM}})\eta_{\text{WIM}} + f_{\text{HIM}}\eta_{\text{HIM}}]N(e^-), \quad (6)$$

where  $f_{\text{HIM}} = N(\text{H II})_{\text{HIM}}/N(\text{H II})$  is the fraction of the H II column associated with the HIM. This value is derived from our estimates of the H II column associated with the hot ISM as discussed in §2.1. While the HIM fraction is model-dependent and poorly constrained observationally, it is only important in this case so far as it affects the mean value of  $\eta$ , which is given in the term in square brackets in Equation 6. We assume 50% uncertainties in  $N(\text{H II})_{\text{HIM}}$ , although its precise value does not affect the total H II column substantially. With this total H II column in hand, we write the total ionization fraction of an ion  $X^j$  as

$$x(X^j)_{\text{total}} = \frac{N(X^j)}{N(\text{H II})}A(X)^{-1}, \quad (7)$$

equivalent to Equation 2. Figure 6 shows the results of this approach as applied to the S ions as well as the high ions  $\text{Si}^{+3}$ ,  $\text{C}^{+3}$ ,  $\text{N}^{+4}$ ,  $\text{O}^{+5}$ . The values are summarized in Table 4. We adopt solar system abundances for these ions. For CNO, these abundances are probably reasonable, since those elements are not depleted by more than a factor of 2 (perhaps less in the hot ISM). Incorporation of Si into the dust phase could lower the gas-phase abundance of Si quite a bit, probably even in the WIM (Howk & Savage 1999). Thus, the ion fraction of  $\text{Si}^{+3}$  could be somewhat higher than shown, perhaps by up to a factor of a few.

## 5. Discussion

We have presented direct measures of the ionization fractions of several ions of S in the WIM of the Milky Way (Figure 4), as well as of the ionization fractions of several metal ions in the integrated (warm and hot) ionized gas of the Milky Way (Figure 6). These figures represent “maps” of the preferred ionization energies in the ionized gas of the Milky Way, showing at what energies we expect to find significant ionization fractions, albeit maps that are slightly skewed by

atomic physics (through varying ionization cross sections and recombination coefficients). In both cases, we find only those ions requiring  $< 35$  eV for their production are present at more than the few percent level up to energies  $\sim 150$  eV. This constrains the sources of ionization for the WIM and the relative mass contributions as a function of temperature for the hotter, collisionally ionized gas (see below).

The WIM shows no absorption from S ions above  $S^{+2}$ . The limits on  $S^{+3}$  and higher absorption are meaningful for several reasons. First, the lack of high ionization S absorption suggests that the only ionization states of S with significant ionization fractions in the WIM are  $S^+$  and  $S^{+2}$ , allowing us to estimate the  $S^+$  ionization fraction (see §4 and Table 3). The  $S^+$  ionization fractions in the WIM along these two sight lines is quite a bit higher than found in classical O-star H II regions, which typically have  $x(S^+) \approx 0.25$  (Haffner et al. 2009), with  $S^{+2}$  being a dominant ion state in those regions. Thus, the WIM has a generally lower ionization state than these H II regions, as noted previously (Haffner et al. 1999, Madsen et al. 2006).

Second, the lack of  $S^{+3}$  (and  $S^{+5}$  toward M 3–vZ 1128) severely limits the amount of high ionization gas produced by the ionization sources for the WIM. The energies required to produce and destroy  $S^+$  are 10.36 eV and 23.33 eV; for  $S^{+2}$  these are 23.33 eV and 34.83 eV. Thus, there is not a significant contribution to the S budget from any ions requiring  $\gtrsim 35$  eV for their production. Essentially all of the S in the WIM is in either  $S^+$  or  $S^{+2}$ . While the ultimate sources of WIM ionization are not precisely known, our measurements require they not produce significant amounts of S ions higher than  $S^{+2}$ . This is of particular importance for understanding the ionization state of He. The energy required to ionize  $S^+$  is close to that required to ionize  $He^0$  (23.33 eV versus 24.59 eV), and the ionization potential of  $S^{+2}$  is well below that required to ionize  $He^+$  (47.22 eV versus 54.42 eV). Thus, the lack of  $S^{+3}$  (probing ionization energies 34.79 to 47.22 eV) thus argues that virutally no  $He^{+2}$  (probing energies 54.42 eV and above) can be present in the WIM.

This conclusion about the lack of  $He^{+2}$  is at odds with the work of Arabadjijs & Bregman (1999), who claim that “there is little room for warm ionized gas of moderate ionization state.” Based on an analysis of the ISM opacity to X-ray emission from distant galaxy clusters, these authors conclude that the fraction of neutral He in the WIM must be very small, with all of the He in either  $He^+$  or  $He^{+2}$ . Since the emission line observations of He I recombination emission only provided a measure of the  $He^+$  ion fraction, this conclusion could not immediately be ruled out by the existing observations. However, our results for the ionization fractions of  $S^{+3}$  and  $S^{+5}$  coupled with measurements of [O III] emission (Madsen et al. 2006, Reynolds 1985b) show that ions requiring  $\gtrsim 35$  eV for creation are trace ions in the WIM. Our limits on S IV give  $x(S^{+3}) < 0.04$  ( $3\sigma$ ) for both sight lines. This ion is destroyed at an energy of  $\sim 47$  eV, well below the energy required to produce  $He^+$ ,  $\sim 55$  eV. The ionization cross sections and recombination coefficients of S and He are not so different that a very high ionization fraction of  $He^{+2}$  could coexist with such

low ionization states of  $S^{+3}$  (e.g., Sembach et al. 2000).

Several models have been developed in an attempt to match the metal ion emission from the WIM. Most of these are 1D models relying on photons from OB stars to provide the ionization (e.g., Mathis 1986, 2000; Domgorgen & Mathis 1994, Sembach et al. 2000, Elwert & Dettmar 2005). These are necessarily simplified models that often assume a single temperature stellar atmosphere and very basic geometry, but include a great deal of atomic physics. Because many of these are largely concerned with matching the emission lines, which are temperature dependent, they do not all discuss directly the metal ion fractions in a way that is appropriate for comparison with the absorption line-derived results presented in this work. Sembach et al. (2000) attempted to model the WIM ionization using a series of 1D models within Cloudy. They specifically tailored their models to assess the impact of the WIM on absorption line measurements. Their recommended composite model gives  $x(S^+) = 0.81$  and  $x(S^{+2}) = 0.18$ . The  $S^{+2}$  fraction, in particular, is lower by factors of 2 to 3 than our observations imply. Indeed, Howk et al. (2006) noted that applying the Sembach et al. (2000) models to the M 3–vZ 1128 sight line did not produce results consistent with the full abundance determination for sulfur (underestimating the total S abundance by -0.4 dex). The sign of this result implies the ratio  $x(S^+)/x(S^{+2})$  in the Sembach et al. models is too large, consistent with our determinations.

More recent models have considered the modification of the radiation field as it propagates through the ISM (e.g., Wood & Mathis 2004, Giammanco et al. 2004). The absorption of some radiation as it passes through the ISM will remove photons just above 1 Rydberg, “hardening” the H-ionizing photons as  $E \approx 1$  Ryd photons are removed while higher energy photons see less opacity. However, this will tend to increase the  $S^+$  ion fractions compared with  $S^{+2}$ , since the former is created by unabsorbed  $E < 1$  Ryd photons while the radiation field is diminished at the energy required to create  $S^{+2}$  (Hoopes & Walterbos 2003). However, this is true only when keeping all else constant. Elwert & Dettmar (2005) attempted to model the run of [S II] emission with height above the Perseus Arm observed by Haffner et al. (1999), following the propagation of radiation through the ISM with height. However, while their models do produce significantly higher  $S^+$  ion fractions well above the plane (and hence are able to match the run of [S II] emission at heights  $z > 1$  kpc above the Perseus Arm), they produce much lower  $S^+$  ion fractions at low heights. Their models have  $x(S^+) = 0.2$  to  $0.5$ , with the ion fraction increasing with height up to  $z \sim 2$  kpc (see their Figure 5). Integrating their  $S^+$  ionization fractions vertically through an assumed exponential WIM distribution with a 1 kpc scale height (e.g., Haffner et al. 1999) gives a mean  $\langle x(S^+) \rangle = 0.28$ , lower by a factor of 2 than the value implied by our observations. A lower latitude sight line through such a model (approximating that to M 5–ZNG 1) would yield an even lower mean ionization fraction. The majority of the S in these models is likely in  $S^{+2}$  at  $z \lesssim 1$  kpc, which dominates the column density of the distribution. The  $S^{+2}$  ion fractions in these models are significantly higher than our measurements imply.



We are not aware of significant constraints on the  $S^{+2}$  ionization fraction from emission line observations that could have been used to guide these earlier models. The emission line diagnostics also have an additional dependence on temperature that can mask mismatches between the model and WIM ionization fractions. Our measurements provide complementary constraints for models of the WIM. The causes of the discrepancies between the two models discussed above and the ionization fractions measured here are unknown at this point, but may include inappropriate choice of ionizing spectra, effects associated with the 3D structure of the gas and radiative transfer, and the lack of appropriate heating sources (which affects the match with emission line diagnostics, but not the absorption line diagnostics here). The ionizing spectrum is likely to be quite complex with multiple types of sources contributing. While it is almost certainly dominated by O star radiation (Haffner et al. 2009), that radiation is processed by intervening absorption and there may be contributions from other sources such as stellar remnants (e.g., Bregman & Harrington 1986, Rand et al. 2011) and cooling radiation from hot gas and transition-temperature interfaces (Slavin et al. 2000).

We note that the conditions in the WIM near the sun may be somewhat different than those seen in other galaxies, where observations of the diffuse ionized gas (DIG) often trace layers brighter than the WIM of the Milky Way (Haffner et al. 2009). In particular, Rand et al. (2011) have recently used *Spitzer* observations of the [Ne III]/[Ne II] ratio to show the ratio of  $Ne^{+2}/Ne^{+}$  is increasing with height above the plane. Because these emission lines are not very sensitive to excitation in the way the optical forbidden lines can be, this is a robust measure of the relative importance of these Ne ions. Observations of [O III] emission also find some galaxies show higher  $O^{+2}$  ionization fractions than implied by the WHAM measurements of the Milky Way. Collins & Rand (2001) study, for example, showed that  $O^{+2}$  could be the dominant ionization state of O in the extraplanar DIG of NGC 5775 and UGC 10288. One concern with comparing the Milky Way and these other galaxies is the difference in the properties of the observed DIG layers compared with the Milky Way’s WIM. The former tend to be quite bright compared with the WIM and are observed at projected radii well within the solar circle in most cases. However, this is suggestive that the results found here may not apply across all galaxies and even over all positions within the Milky Way.

The ionization fractions shown in Figure 6 demonstrate the importance of the WIM in the strong peak between  $\sim 10$  and 35 eV, but they also shed light on the conditions in the hotter ionized gas of the Milky Way. With the exception of  $S^{+}$  and  $S^{+2}$ , none of the ions in Figure 6 exceeds an ionization fraction of 0.05. The very low ionization fractions of the high ions  $Si^{+3}$ ,  $C^{+3}$ ,  $N^{+4}$ ,  $O^{+5}$  have two causes. First, none of these Li-like ions (or Na-like in the case of Si IV) is expected to be the dominant ionization state at any temperature, having peak ionization fractions of  $\approx 0.25$  (Gnat & Sternberg 2007). However, the values seen in Figure 6 are an order of magnitude or more lower than this. The low ionization fractions for these high ions reflect the relatively small contribution

of gas in the transition temperature regime with  $T \sim 7 \times 10^4 - 4 \times 10^5$  K to the total ionized gas content of the Milky Way. This is understandable: gas at these temperatures is at the peak of the interstellar cooling curve and radiates its energy very quickly, thereby cooling very quickly through this temperature regime. Thus, while the total mass budget of such transition temperature gas is not large compared with the WIM or the hotter HIM (see below), it is very important energetically. The mass flux or cooling flux through this regime is likely to be quite important. In fact, the ion fractions for these high ions include contributions from such transition-temperature gas as well as the  $\sim 40\%$  of such gas that is at  $T < 7 \times 10^4$  K, representing matter that has already cooled and is out of ionization equilibrium or gas that is photoionized by the radiatively cooling HIM (Lehner et al. 2011).

Figure 6 hints that there are likely to be two peaks in the total ionization fractions in the ionized gas of the Milky Way. One is associated with the WIM and traced by ions that probe the energy range  $E \sim 10$  to  $35$  eV, as demonstrated by the large ionization fractions of  $S^+$  and  $S^{+2}$ . This gas is predominantly photoionized and warm. The second peak is unseen in this plot, since we have no ions probing energies  $E \gtrsim 140$  eV. The gas associated with the hot ISM at  $T \gtrsim 4 \times 10^5$  K (above that typically probed by O VI) will be traced in O by  $O^{+6}$  and  $O^{+7}$ ; such gas will be traced in S by  $S^{+6}$  and higher (e.g., Sutherland & Dopita 1993, Gnat & Sternberg 2007). While we cannot directly probe these ionization states along these sight lines, we can strongly limit their combined contribution. Summing the ionization fractions of  $S^+$  and  $S^{+2}$ , we have  $x(S^+) + x(S^{+2}) \approx 0.80 \pm 0.10$  along both the M 3 and M 5 sight lines. Thus, the combined fractions of all other ionization states represent only  $\approx (20 \pm 10)\%$  of the total S in these directions. The second peak in the ionization fractions of S ions should trace the high temperature HIM at a few hundred eV and have a magnitude of  $\lesssim 0.2$ . Figure 7 shows a plot of our derived ionization fractions supplemented by a calculation of sulfur ionization fractions for a hot, collisionally-ionized phase with  $T = 2 \times 10^6$  K (e.g., Yao & Wang 2006). The hot phase ion fractions are from a Cloudy (Ferland et al. 1998) calculation assuming collisional ionization equilibrium (CIE) and have been normalized to sum to 20% of the total (although the total for these high energies may be somewhat less). Thus, this figure shows a map of the expected energies at which one expects to find ions within the ionized medium of the Milky Way. The distribution in the highest ions depends on the assumed temperature of the HIM, but the other ions now have firmly measured ionization fractions along these two sight lines.

The very low ion fractions of the high ions observable in the UV (esp.  $O^{+5}$ ) have implications beyond the Galaxy. The strong O VI doublet is among the best tracers of highly-ionized gas in galaxy halos over all redshifts (Prochaska et al. 2011, Tumlinson et al. 2011). Studies of this sort that attempt to make estimates of the mass of gaseous galaxy halos seen in absorption, correcting the O VI columns based upon an assumed ionization fraction from collisional ionization models (e.g., Gnat & Sternberg 2007). In these cases, the typical ionization fraction adopted is  $x(O^{+5}) \lesssim 0.2$  (Gnat & Sternberg 2007, Sutherland & Dopita 1993). This may be the ionization

fraction in the O VI-bearing gas at the temperatures where O VI peaks in abundance, and this gas represents a small fraction of the total, as we have discussed above. However, if one wishes to use O VI to calculate the total mass of ionized gas or the mass of hot ionized gas (e.g.,  $T \gtrsim 10^5$  K in this case), our results suggest some caution may need to be used, as a much lower mean ionization fraction is suggested for our two sight lines. In the two sight lines studied here, we find  $x(\text{O}^{+5}) \lesssim 0.01$  when considering the warm and hot ionized gas together. The O VI along these sight lines represents  $\lesssim 5\%$  of the oxygen in the hot gas. The applicability of our results, which probe the thick disk of the Milky Way within  $z \lesssim 10$  kpc of the midplane, to much different environments is unclear. Many studies in which such corrections are important probe galaxy halos at several tens of kpc impact parameter from galaxies (e.g., Prochaska et al. 2011, Tumlinson et al. 2011) or probe the outskirts of HVCs (e.g., Fox et al. 2006, Sembach et al. 2003), which may have different ionization conditions than the gas in the Milky Way thick disk.

## 6. Summary

We have presented a method for studying the ion fractions of metal ions in the ionized gas of the Galaxy, expanding upon the method presented by Howk et al. (2006) for measuring elemental abundances. We make use of unique sight lines toward globular clusters containing both UV bright stars (for measuring the metal ions) and pulsars (for measuring the electron column density). We apply this method to study the ionization of the ionized gas toward M 3–vZ 1128 and M 5–ZNG 1, both of which probe extended paths through the Galactic thick disk or halo, providing estimates for the ionization fractions of  $\text{S}^0$ ,  $\text{S}^+$ ,  $\text{S}^{+2}$ ,  $\text{S}^{+3}$ , and  $\text{S}^{+5}$  in the WIM. We also assess the ionization fractions integrated through the warm and hot ISM of the Milky Way.

Our principal conclusions based on this analysis are as follows.

1. The only ions with significant ionization fractions in the WIM are those with ionization potentials  $\lesssim 35$  eV. We find  $\text{S}^{+2}$  makes up a substantial portion of the WIM sulfur, with ionization fractions  $x(\text{S}^{+2}) = 0.33 \pm 0.07$  and  $0.47 \pm 0.09$  toward M 3 and M 5, respectively.
2. We limit the contribution of  $\text{S}^{+3}$  and higher ionization states of sulfur, with  $3\sigma$  upper limits  $x(\text{S}^{+3}) < 0.06$  for both of our sight lines. Given the lack of higher ionization states in the WIM, the ionization fractions of  $\text{S}^+$  and  $\text{S}^{+2}$  represent the vast majority of the WIM sulfur. Assuming these add to unity, we derive  $x(\text{S}^+) = 0.67 \pm 0.07$  and  $0.53 \pm 0.09$  toward M 3 and M 5, respectively. These numbers are in good agreement with emission-line derived  $\text{S}^+$  ion fractions (Haffner et al. 1999, Madsen et al. 2006).
3. Existing, simplified photoionization models for the WIM produce S ion fractions that can differ by factors of 2 from our estimates, with various models under- or over-producing  $\text{S}^{+2}$ .

These models are largely constructed to match emission line measurements, which provide access to a narrower range of ions than our measurements. The lack of higher ionization states in the WIM rules out the conclusion of Arabadjis & Bregman (1999) that much of the He in the WIM is in the form of  $\text{He}^{+2}$  and limits the hardness of the radiation field responsible for ionizing the WIM.

4. We show that the ionized gas column density (and hence mass) along these two sight lines is dominated by warm photoionized gas ( $T \sim 10^4$  K) favoring ionization states with ionization energies  $E \sim 10$  to 35 eV and a hot ionized phase ( $T \gtrsim 4 \times 10^5$  K) favoring energies of a few hundred eV. The warm phase contains  $\sim 80\%$  of the total ionized gas column, and the hot phase  $< 20\%$ . The important tracer O VI probes only a small fraction of the ionized gas along the sight line with  $x(\text{O}^{+5}) < 0.01$ .

Financial support was provided through NASA grants HST-GO-9150.03-A and HST-GO-9410.03-A through Space Telescope Science Institute, which is operated by the Association of Universities for Research in Astronomy, Inc., under NASA contract NAS5-26555. We thank N. Lehner, J.X. Prochaska, R. Rand, and J. Tumlinson for useful comments and discussions.

## REFERENCES

- Arabadjis, J.S., & Bregman, J.N. 1999, *ApJ*, 510, 806
- Asplund, M. Grevesse, N., Sauval, A.J., & Scott, P. 2009, *ARAA*, 47, 481
- Bregman, J.N., & Harrington, J.P. 1986, *ApJ*, 309, 833
- Collins, J. A., & Rand, R. J. 2001, *ApJ*, 551, 57
- Domgörgen, H. & Mathis, J.S. 1994, *ApJ*, 428, 647
- Dove, J.B. & Shull, J.M. 1994, *ApJ*, 430, 222
- Dove, J.B., Shull, J.M., & Ferrara, A. 2000, *ApJ*, 531, 2, 846
- Elwert, T., & Dettmar, R.-J. 2005, *ApJ*, 632, 277
- Flores-Fajardo, N., Morisset, C., Stasinska, G., & Binette, L. 2011, *MNRAS*, 415, 2182
- Fox, A.J., Savage, B.D., & Wakker, B.P. 2006, *ApJS*, 165, 229
- Freire, P.C.C., Wolszczan, A., van den Berg, M., & Hessels, J.W.T 2008, *ApJ*, 679, 1433
- Gaensler, B.M., Madsen, G.J., Chatterjee, S., & Mao, S.A. 2008, *PASA*, 25, 184
- Giammanco, C., Beckman, J. E., Zurita, A., & Relaño, M. 2004, *A&A*, 424, 877

- Gnat, O., & Sternberg, A. 2007, *ApJS*, 168, 213
- Gómez, G.C., Benjamin, R.A., & Cox, D.P. 2001, *ApJ*, 122, 908
- Haffner, L.M. 1999, Ph.D. thesis, Univ. Wisconsin, Madison
- Haffner, L.M., Reynolds, R.J., & Tufte, S.L. 1999, *ApJ*, 523, 223
- Haffner, L.M., Dettmar, R.J, Beckman, J.E., et al. 2009, *Reviews of Modern Physics*, 81, 969
- Hausen, N.R., Reynolds, R.J., & Haffner, L.M. 2002, *AJ*, 124, 3336
- Hessels, J.W.T., Ransom, S.M., Stairs, I.H., Kaspy, V.M., & Freire, P.C.C 2007, *ApJ*, 670, 363
- Hoffman, T.L., Leib, S., Pauldrach, A.W.A., Lesch, H., Hultzsch, P.J.N., & Birk, G.T. 2012, *A&A*, in press (arXiv:1206.0394)
- Hoopes, C.G., & Walterbos, R.A.M. 2003, *ApJ*, 586, 902
- Howk, J.C., & Savage, B.D. 1999, *ApJ*, 517, 746
- Howk, J.C., Savage, B.D., Fabian, D. 1999, *ApJ*, 525, 253
- Howk, J.C., Savage, B.D., Sembach, K.R., & Hoopes, C.G. 2002, *ApJ*, 572, 264
- Howk, J.C., Sembach, K.R., & Savage, B.D. 2003, *ApJ*, 586, 249
- Howk, J.C., Sembach, K.R., & Savage, B.D. 2006, *ApJ*, 637, 333
- Hoyle, F. & Ellis, G.R.A 1963, *AuJPh*, 16, 1
- Hubeny, I. & Lanz, T. 1995, *ApJ*, 439, 875
- Kalberla, P.M.W., Burton, W.B., Hartmann, D., Arnal, E.M., Bajaja, E., Morras, R., & Pöppel, W.G.L 2005, *A&A*, 440, 775
- Lehner, N., Zech, W.F., Howk, J.C., & Savage, B.D. 2011, *ApJ*, 727, 46
- Madsen, G.J. 2004, PhD Thesis, University of Wisconsin–Madison
- Madsen, G.J., Reynolds, R.J., & Haffner, L.M. 2006, *ApJ*, 652, 401
- Mathis, J.S. 1986, *ApJ*, 301, 423
- Mathis, J.S. 2000, *ApJ*, 544, 347
- Miller, W.W., III, Cox, D.P. 1993, *ApJ*, 417, 579
- Morton, D.C. 2003, *ApJS*, 149, 205
- Bostroem, K. & Proffitt, C., 2001, “STIS Data Handbook”, Version 6.0, (Baltimore:STScI)
- Prochaska, J.X., Weiner, B., Chen, H.-W., Mulchaey, J., & Cooksey, K. 2011, *ApJ*, 740, 91
- Rand, R. J., Wood, K., Benjamin, R. A., & Meidt, S. E. 2011, *ApJ*, 728, 163
- Reynolds, R.J. 1985a, *ApJ*, 294, 256

- Reynolds, R.J. 1985b, *ApJ*, 298, L27
- Reynolds, R.J. 1988a, *AJ*, 96, 670
- Reynolds, R.J. 1988b, *ApJ*, 333, 341
- Reynolds, R.J. 1989, *ApJ*, 345, 811
- Reynolds, R.J. 1993, in *Back to the Galaxy*, ed. S. Holt & F. Verter (New York: American Institute of Physics), 156
- Reynolds, R.J., Hausen, N.R., Tufte, S.L., & Haffner, L.M. 1998a, *ApJ*, 494, L99
- Reynolds, R.J., & Tufte, S.L. 1995, *ApJ*, 439, L17
- Reynolds, R.J., Hausen, N.R., Tufte, S.L., & Haffner, L.M. 1998a, *ApJ*, 494, L99
- Reynolds, R.J., Tufte, S.L., Haffner, L.M., Jaehing, K., & Percival, J.W. 1998b, *PASA*, 15, 14
- Reynolds, R.J., Sterling, N.C., Haffner, L.M., & Tufte, S.L. 2001, *ApJ*, 548, L221
- Savage, B.D. & Sembach, K.R. 1991, *ApJ*, 379, 245
- Savage, B.D., Sembach, K.R., Wakker, B.P., et al. 2003, *ApJ*, 146, 125S
- Sciama, D.W. 1998, *ApJL*, 505, L35
- Sembach, K.R. & Savage, B.D. 1992, *ApJS*, 83, 147
- Sembach, K.R., Howk, J.C., Ryans, R.S.I., & Keenan, F.P. 2000, *ApJ*, 528, 310
- Sembach, K.R., Wakker, B.P., Savage, B.D., et al. 2003, *ApJS*, 146, 165
- Slavin, J.D., McKee, C.F., & Hollenbach, D.J. 2000, *ApJ*, 541, 218
- Sonneborn, G., André, M.K., Oliveira, C., et al. 2002, *ApJS*, 140, 51
- Sutherland, R.S. & Dopita, M.A. 1993, *ApJS*, 88, 253
- Tumlinson, J., Thom, C., Werk, J.K., et al. 2011, *Science*, 334, 948
- Tufte, S.L. 1997, Ph.D. thesis, Univ. Wisconsin, Madison
- Wakker, B.P., Kalberla, P.M.W., van Woerden, H., de Boer, K.S., & Putman, M.E. 2001, *ApJS*, 136, 537
- Wakker, B.P., Savage, B.D., Sembach, K.R., et al. 2003 *ApJ*, 146, 1
- Wood, K. & Mathis, J.S. 2004, *RAS*, 353, 1126
- Wood, K., Hill, A.S., Joungh, M.R., Mac Low, M., Benjamin, R.A., Haffner, L.M., Reynolds, R.J., & Madsen, G.L. 2010, *ApJ*, 721, 1397
- Yao, Y. & Wang, Q.D. 2005, *ApJ*, 624, 751

Yao, Y., Wang, Q.D., Hagihara, T., Mitsuda, K., McCammon, D., & Yamasaki, N.Y. 2009, ApJ, 690, 143

Zech, W.F., Lehner, N., Howk, J.C., Van Dyke Dixon, W., & Brown, T.M. 2008, ApJ, 679, 460

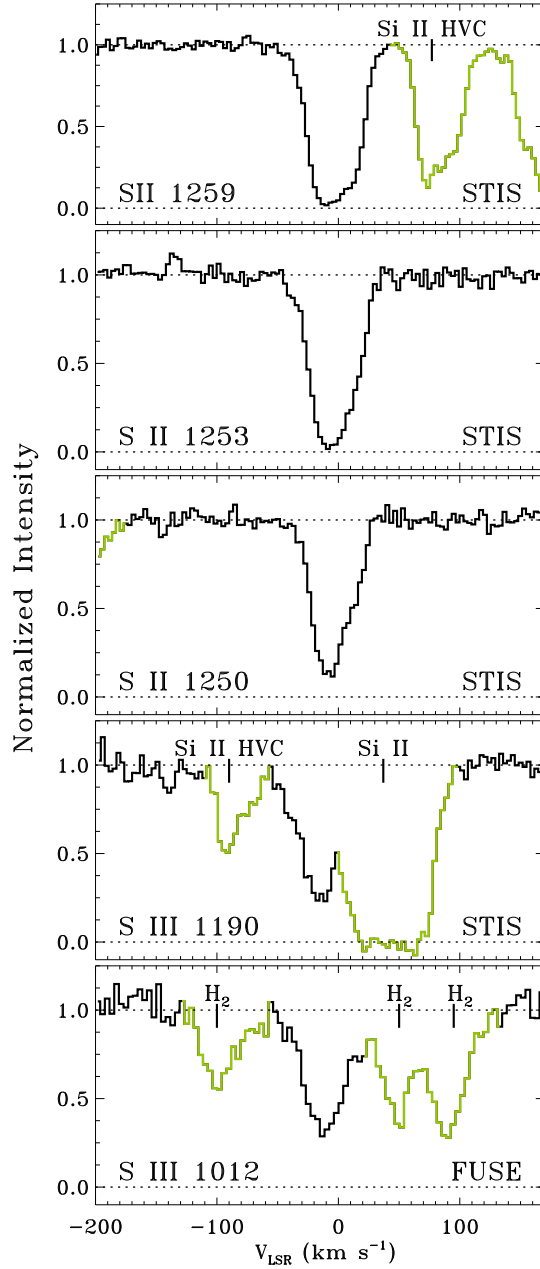


Fig. 1.— Absorption line profiles of S II  $\lambda\lambda$  1250.584, 1253.811, 1259.519, and S III  $\lambda$  1190.208 from STIS E140M observations as well as S III  $\lambda$  1012.495 from *FUSE* observations of M5-ZNG1. The lighter colored portion of the spectra are interloping lines. The *FUSE* data are shown with a binned pixel size of  $3.84 \text{ km s}^{-1}$ , giving  $\sim 5$  pixels per resolution element. The STIS data are shown with their native pixels, that is  $3.22 \text{ km s}^{-1}$ , or  $\sim 2.3$  pixels per resolution element at these wavelengths (Proffitt et al. 2002).



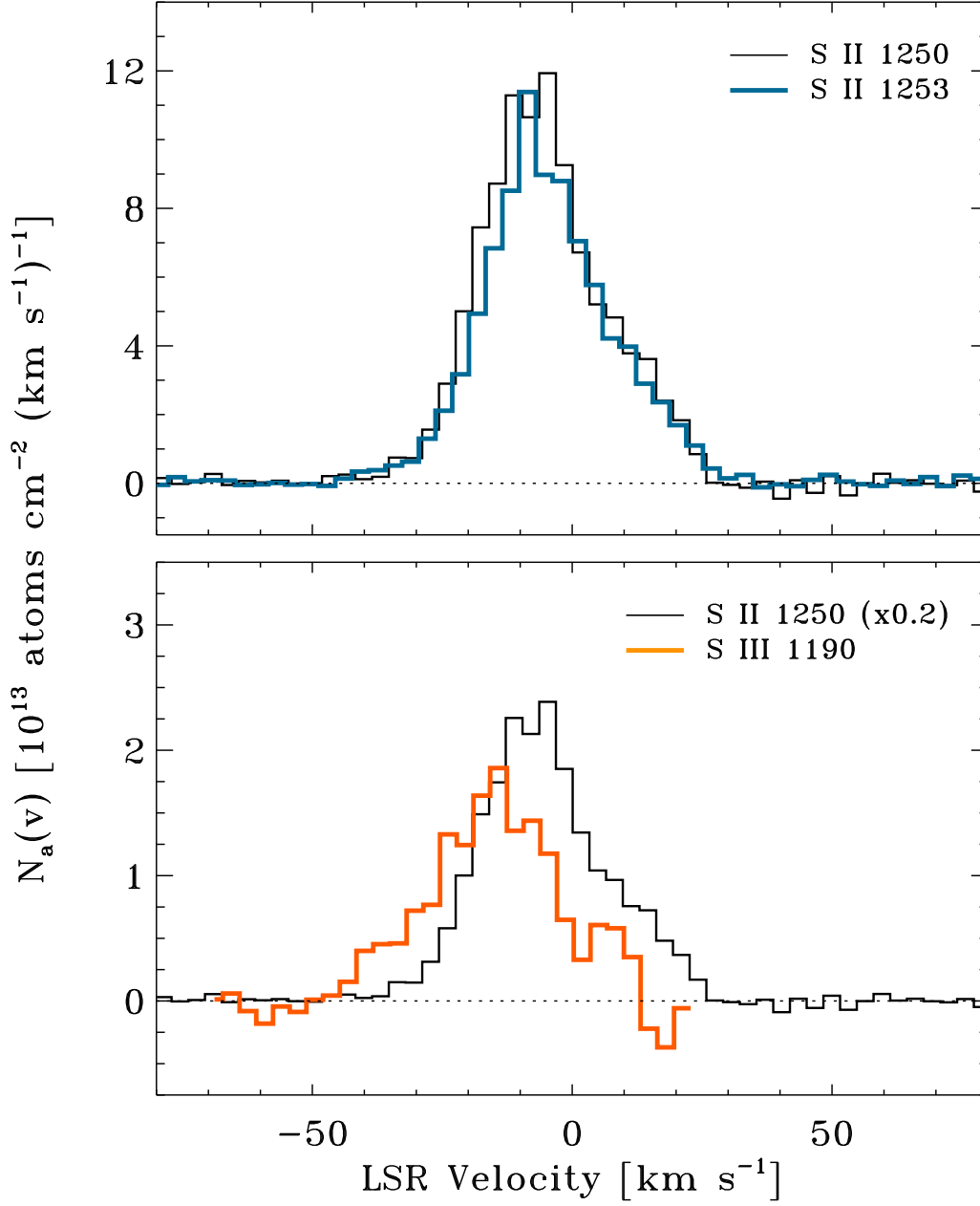


Fig. 2.— Comparison of the apparent column density profiles for S II  $\lambda 1250.584$ ,  $1253.811$ , and S III  $\lambda 1190.208$  from STIS E140M observations. The top panel is a comparison of the two S II profiles. The discrepancy between the two profiles is due to the presence of unresolved saturation. The lower panel compares the S II line at  $1250.54 \text{ \AA}$  with the S III line at  $1190.208 \text{ \AA}$ . The S III profile has been “cleaned” of Si II contamination.

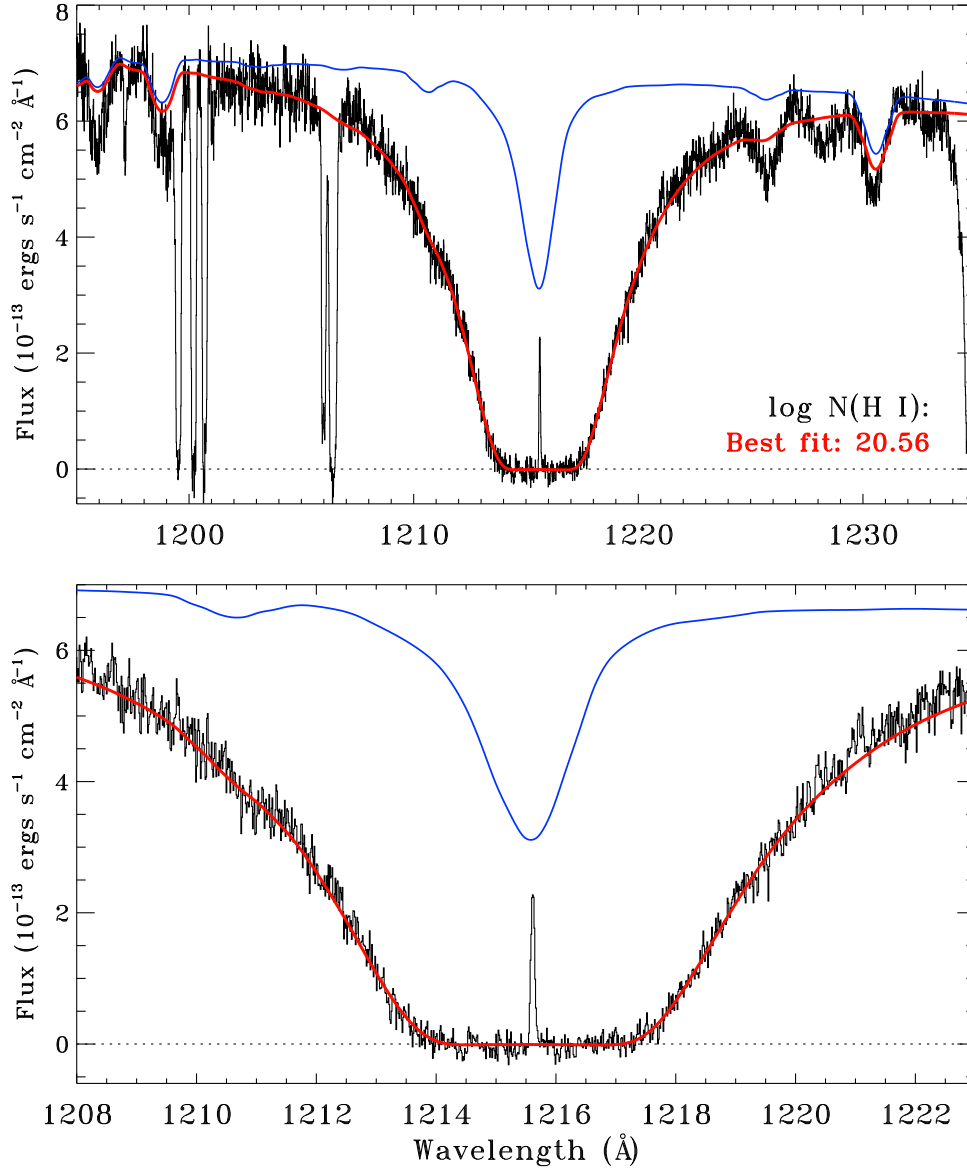


Fig. 3.— Two views of the STIS E140M spectrum of the Lyman- $\alpha$  absorption profile toward M 5–ZNG 1. Both stellar and interstellar absorption contribute to this profile. The estimated stellar profile is shown as the thin blue line and has been shifted to  $v_{\text{LSR}} = +65.7$  km s $^{-1}$  to match the observed positions of stellar absorption lines in the STIS spectrum. The best fit to the interstellar and stellar absorption profile is shown in red, corresponding to an interstellar column density  $\log N(\text{H I}) = 20.47 \pm 0.02$ . The sharp line in the center of the Lyman- $\alpha$  absorption trough is geocoronal emission.

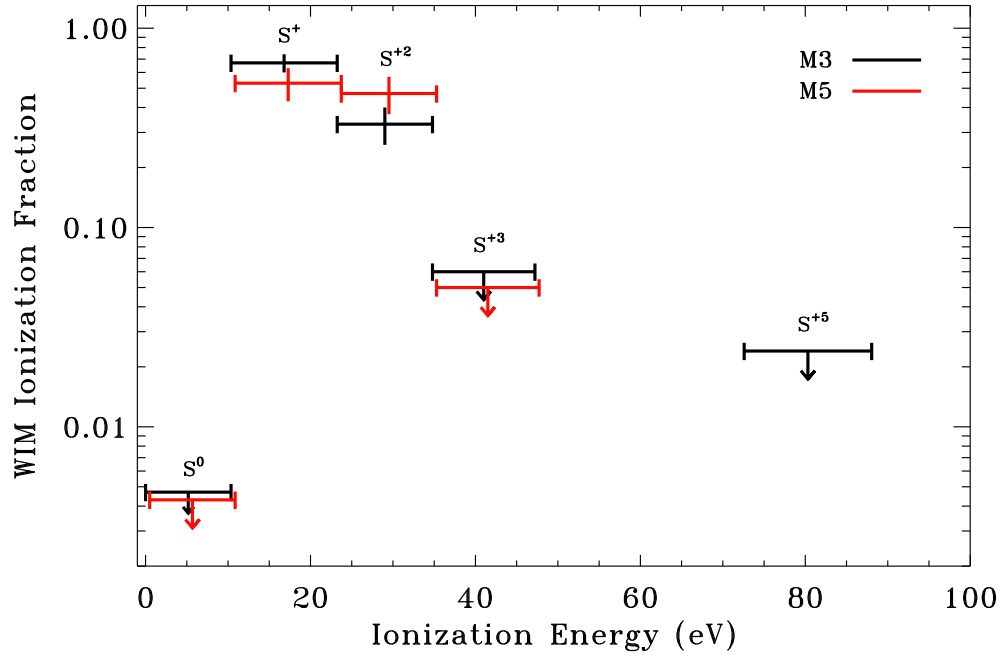


Fig. 4.— The ionization fractions,  $x(X^j)$ , of S ions in the WIM as a function of ionization energies for the M 3 (black) and M 5 (red) sight lines. The horizontal extent of the bars for each ion span the range of energies required to create it, from the next lower ionization state, and destroy it, creating the next higher ionization state (i.e., the ionization energies). The M 5 ionization energies are offset by 0.5 eV for clarity.

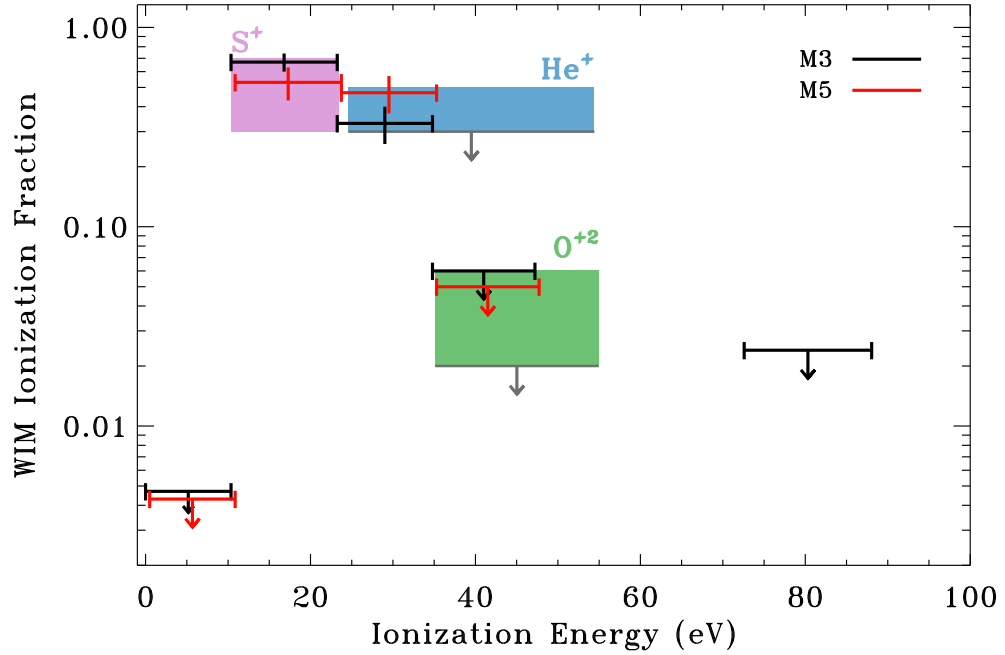


Fig. 5.— A comparison of emission and absorption line constraints on ionization fractions for several ions in the WIM. The ionization fractions derived here for S ions are shown for the M 3 (black) and M 5 (red) sight lines as in Figure 4. The shaded regions denote the range of values seen by emission line constraints on the ionization fractions of  $S^+$  (Haffner et al. 1999, Madsen et al. 2006 as summarized in Haffner et al. 2009),  $O^{+2}$  (Madsen et al. 2006, Reynolds & Tufte 1995), and  $He^+$  (Madsen et al. 2006, Madsen 2004, Reynolds 1985b). We have excluded the values associated with the northern filament studied by, e.g., Madsen et al. (2006) that seems to show higher ionization fractions for  $O^{+2}$  and  $He^+$  than typically found in the diffuse WIM. The lowest upper limits on the emission constraints are shown with downward facing arrows.

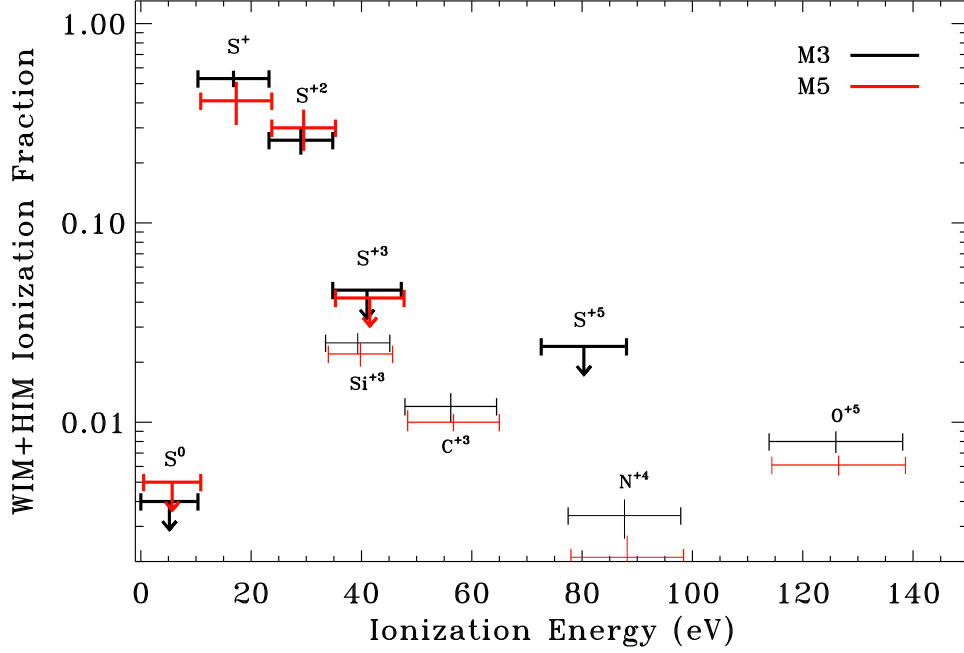


Fig. 6.— The ionization fractions integrated over all of the ionized gas (WIM+HIM) of the Milky Way for several metal ions as a function of ionization energies for the M 3 (black) and M 5 (red) sight lines. This plot differs from Figure 4 in that it applies to both the WIM and HIM. The results are tabulated in Table 4. The mass of ionized gas (at least along these sight lines) is dominated by WIM gas traced by ions in the range  $\sim 10$  to  $35$  eV and by a hotter component with  $T > 4 \times 10^5$  K probed by ions with higher ionization energies than probed by the available UV transitions. Together the WIM ions account for 80% of the total, implying that ions tracing the high temperature phase cannot represent more than  $\sim 20\%$  of the total contribution to any metal. Gas with temperatures in the range a few  $\times 10^4$  K to  $\sim 4 \times 10^5$  K contributes very little to the total mass budget, as discussed in §5.

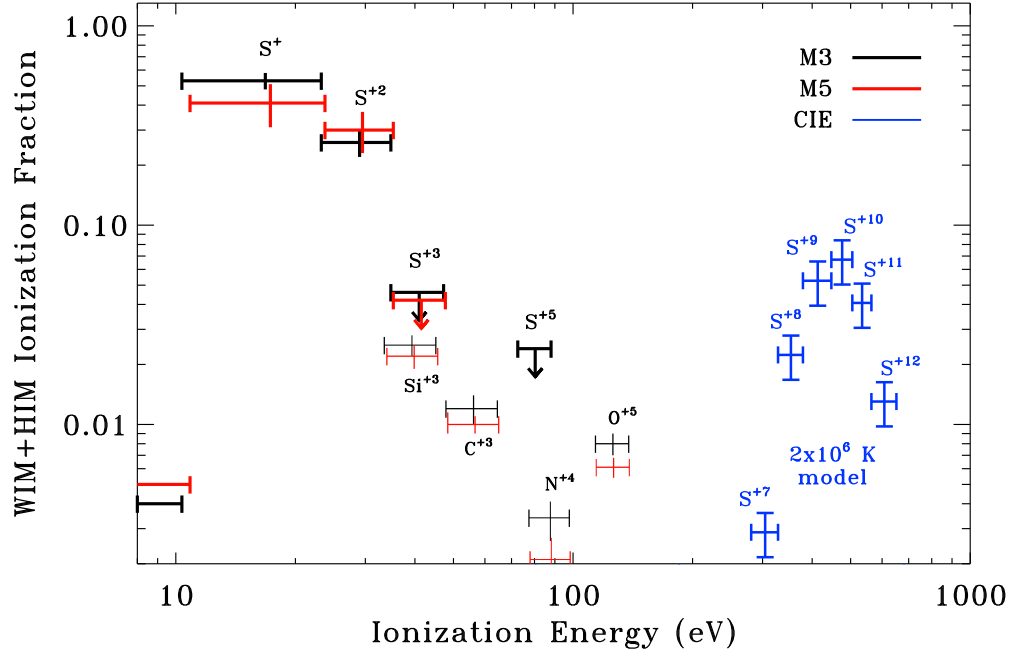


Fig. 7.— The ionization fractions for the total ionized gas (WIM+HIM) of the Milky Way, as Figure 6, for several metal ions as a function of ionization energies (plotted on a log scale here), including CIE models for S ions in the hot ionized phase (blue). The CIE models assume  $T = 2 \times 10^6$  K (e.g., Yao & Wang 2006) for the HIM and have been normalized to contribute  $(20 \pm 5)\%$  of the total ionization fraction, although the contribution could be somewhat lower. The ionization fractions of all the S ions in this figure sums to unity. This plot represents a map of the energies at which we expect significant ionization fraction contributions over all species. The distribution of S ions in CIE will, of course, depend on the assumed temperature.

Table 1. Adopted Column Densities Toward M 3 and M 5

| Species | M 3 - vZ 1128           |                   | M 5 - ZNG 1             |                   |
|---------|-------------------------|-------------------|-------------------------|-------------------|
|         | $\log N$                | Ref. <sup>a</sup> | $\log N$                | Ref. <sup>a</sup> |
| H I     | $19.98 \pm 0.03$        | 1                 | $20.57 \pm 0.03$        | 4                 |
| $e^-$   | $19.91 \pm 0.01$        | 2                 | $19.96 \pm 0.01$        | 2,5               |
| C IV    | $14.39 \pm 0.03$        | 4                 | $14.38 \pm 0.02$        | 4                 |
| N V     | $13.25^{+0.07}_{-0.09}$ | 4                 | $13.10^{+0.10}_{-0.14}$ | 4                 |
| O VI    | $14.49 \pm 0.03$        | 3                 | $14.41 \pm 0.02$        | 4                 |
| Si IV   | $13.80 \pm 0.02$        | 4                 | $13.79 \pm 0.02$        | 4                 |
| S I     | $< 12.7 (3\sigma)$      | 3                 | $< 12.7 (3\sigma)$      | 4                 |
| S II    | $15.28 \pm 0.02$        | 3                 | $15.59 \pm 0.10$        | 4                 |
| S III   | $14.47 \pm 0.03$        | 3                 | $14.66 \pm 0.02$        | 4                 |
| S IV    | $< 13.7 (3\sigma)$      | 3                 | $< 13.7 (3\sigma)$      | 4                 |
| S VI    | $< 13.4 (3\sigma)$      | 3                 | ...                     | ...               |

<sup>a</sup>References: (1) Howk et al. 2006 ; (2) Hessels et al. 2007; (3) Howk et al. 2003; (4) This Work; (5) Freire et al. 2008.

Table 2. Derived Interstellar Parameters Toward M 3 and M 5

| Quantity                     | M 3              | M 5              |
|------------------------------|------------------|------------------|
| $\log N(e^-)$                | $19.91 \pm 0.01$ | $19.96 \pm 0.01$ |
| $\log N(\text{H II})_{HIM}$  | $19.20 \pm 0.18$ | $18.93 \pm 0.18$ |
| $\log N(\text{H II})_{WIM}$  | $19.79 \pm 0.06$ | $19.83 \pm 0.06$ |
| $\log N(\text{H})^a$         | $20.24 \pm 0.03$ | $20.66 \pm 0.02$ |
| $N(\text{H II})/N(\text{H})$ | $0.45 \pm 0.09$  | $0.19 \pm 0.03$  |
| $\log A(\text{S})^b$         | $-4.86 \pm 0.04$ | $-5.00 \pm 0.10$ |
| [S/H]                        | $-0.01 \pm 0.04$ | $-0.15 \pm 0.10$ |

<sup>a</sup>The total hydrogen column density, including contributions from both warm and hot gas, i.e., including the ionized gas associated with the HIM.

<sup>b</sup>The sulfur abundance is derived excluding the H II column from the HIM. Thus, the hydrogen reference columns for comparison with the summed S ion column densities are  $\log N(\text{H}) = 20.20 \pm 0.03$  and  $20.64 \pm 0.02$  for M 3 and M 5, respectively.



Table 3. WIM Sulfur Ionization Fractions<sup>a</sup>

| Quantity           | M 3                 | M 5 <sup>b</sup>    |
|--------------------|---------------------|---------------------|
| $x(\text{S}^0)$    | $< 0.006 (3\sigma)$ | $< 0.005 (3\sigma)$ |
| $x(\text{S}^+)$    | $0.67 \pm 0.07^c$   | $0.53 \pm 0.09^c$   |
| $x(\text{S}^{+2})$ | $0.33 \pm 0.07$     | $0.47 \pm 0.09$     |
| $x(\text{S}^{+3})$ | $< 0.06 (3\sigma)$  | $< 0.05 (3\sigma)$  |
| $x(\text{S}^{+5})$ | $< 0.03 (3\sigma)$  | $\dots$             |

<sup>a</sup>The ionization fractions are  $x(X^j) \equiv N(X^j)/N(X)$ . We assume  $x(\text{H}^+) = 0.95 \pm 0.05$  in deriving these values (see text).

<sup>b</sup>We adopt the abundance towards M 3 for the ionization fraction calculations. If one adopts the less well-determined value derived for M 5, the result for  $\text{S}^{+2}$ , for example, is  $x(\text{S}^{+2}) = 0.67 \pm 0.19$ .

<sup>c</sup>The  $\text{S}^+$  ion fractions are not measured directly; instead they are derived assuming  $x(\text{S}^+) + x(\text{S}^{+2}) = 1$  (see text).

Table 4. Total (WIM+HIM) Ionization Fractions<sup>a</sup>

| Quantity            | M 3                            | M 5                           |
|---------------------|--------------------------------|-------------------------------|
| $x(\text{S}^0)$     | $< 0.005 (3\sigma)^c$          | $< 0.004 (3\sigma)^c$         |
| $x(\text{S}^+)$     | $0.53 \pm 0.10^d$              | $0.42 \pm 0.10^d$             |
| $x(\text{S}^{+2})$  | $0.27 \pm 0.04^c$              | $0.38 \pm 0.08^c$             |
| $x(\text{S}^{+3})$  | $< 0.05 (3\sigma)^c$           | $< 0.04 (3\sigma)^c$          |
| $x(\text{S}^{+5})$  | $< 0.02 (3\sigma)^d$           | $\dots$                       |
| $x(\text{C}^{+3})$  | $0.012^{+0.002}_{-0.0008}{}^d$ | $0.10^{+0.001}_{-0.0007}{}^d$ |
| $x(\text{N}^{+4})$  | $0.003 \pm 0.001^e$            | $0.002 \pm 0.002^e$           |
| $x(\text{O}^{+5})$  | $0.008 \pm 0.001^e$            | $0.006 \pm 0.001^e$           |
| $x(\text{Si}^{+3})$ | $0.025 \pm 0.03^e$             | $0.022 \pm 0.003^e$           |

<sup>a</sup>The ionization fractions are  $x(X^j) \equiv N(X^j)/N(X)$ . We assume  $x(\text{H}^+) = 0.95 \pm 0.05$  (see text). For the hottest gas, we expect this fraction to be unity.

<sup>b</sup>We adopt the abundance towards M 3 for the ionization fraction calculations.

<sup>d</sup>The  $\text{S}^+$  ion fractions are not measured directly; instead they are derived assuming  $x(\text{S}^+) + x(\text{S}^{+2}) = 1$  (see text).

<sup>e</sup>Ions higher than  $\text{S}^{+3}$  have an assumed  $x(\text{H}^+) = 1.0$